S2-24

P-34

# Out-of-Plane Properties

Wade C. Jackson
Vehicle Structures Directorate (ARL)


Marc A. Portanova
Lockheed Engineering & Science

## Abstract

This paper summarizes three areas of research which were performed to characterize out-of-plane properties of composite materials. In the first investigation, a series of tests was run to characterize the through-the-thickness tensile strength for a variety of composites that included 2D braids, 2D and 3D weaves, and prepreg tapes. A new test method based on a curved beam was evaluated. Failures were significantly different between the 2D materials and the 3D weaves. The 2D materials delaminated between layers due to out-of-plane tensile stresses while the 3D weaves failed due to the formation of radial cracks between the surface plies caused by high circumferential stresses along the inner radius. The strength of the 2D textile composites did not increase relative to the tapes. Final failure in the 3D weaves was caused by a circumferential crack similar to the 2D materials and occurred at a lower bending moment than in the other materials. The early failures in the 3D weaves were caused by radial crack formation rather than a low through-the-thickness strength. The second investigation focused on the development of a standard impact test method to measure impact damage resistance. The only impact tests that currently exist are compression after impact (CAI) tests which incorporate elements of both damage resistance and damage tolerance. A new impact test method is under development which uses a quasi-static indentation (QSI) test to directly measure damage resistance. Damage resistance is quantified in terms of the contact force to produce a unit of damage where the metric for damage may be area in C-scan, depth of residual dent, penetration, damage growth, etc. A final draft of an impact standard that uses a QSI test method will be presented to the ASTM Impact Task Group on impact. In the third investigation, the impact damage resistance behavior of a variety of textile materials was studied using the QSI test method. In this study, the force where large damage initiates was measured and the delamination size as a function of force was determined. The force to initiate large damage was significantly lower in braids and weaves. The delamination diameter - impact force relationship was quantified using a damage resistance parameter, $Q^*$, which related delamination diameter to impact force over a range of delamination sizes. Using this $Q^*$ parameter to rate the materials, the stitched uniweaves, toughened epoxy tapes, and through-the-thickness orthogonal interlock weave were the most damage resistant.

# Through-the-Thickness Tensile Strength of Textile Composites

Textile composite materials have the potential for better through-the-thickness properties than traditional laminated composites. Traditional laminated composites are very susceptible to delamination from out-of-plane loads that may occur from impact loading or around structural details such as curved geometry, ply drops, or fasteners. With improved through-the-thickness properties, the susceptibility to damage from out-of-plane loads should be greatly reduced.

Textile composites may have a 2D construction where discrete layers are stacked to produce a desired thickness or a 3D construction where a single layer is manufactured to a desired thickness. In the 2D materials, the preform layers are expected to nest snugly together to improve the through-the-thickness properties. In the 3D materials, reinforcement in the thickness direction was specifically included to directly improve these properties.

Through-the-thickness tensile strength is an important material property but is a difficult property to quantify. In laminated composite materials, the through-the-thickness tensile strength can be approximated by the transverse-width strength measured from flat 90° specimens [1]. In textile composites, however, the architecture of the preform is three dimensional with significantly different properties in all directions. In this study, two test methods that incorporate a specimen with a curved test section were used. Through-the-thickness tension is induced in the test section by a moment which attempts to open the curve. One of these test methods uses a curved beam in four-point bending to measure the strength [2]. This method was developed for this test program and was evaluated as part of this investigation

Using these two test methods, a series of tests was run to characterize the through-the-thickness strength for a variety of composites made from textile preforms. Specimens were made from four different 2D braids, six 3D weaves, prepreg fabrics, and from unidirectional tape specimens. For both loading configurations, the data were reduced using an elasticity solution for anisotropic curved beams.

## Materials

A variety of textile and prepreg tape materials were used in this investigation. All specimens were manufactured with Hercules AS4 carbon fibers and similar resins. For comparison purposes, a toughened epoxy (8551-7) was also used to make tape specimens. All tape specimens were manufactured using prepregs of AS4/3501-6 (24 & 48 ply) or AS4/8551-7 (25 & 48 ply). The 2D braided and 3D woven preforms were impregnated with Shell RSL-1895/W epoxy resin using the resin transfer molding (RTM) process [3]. The 1895/W system was developed for RTM and has similar properties to 3501-6 epoxy.

The 2D braids were formed on cylindrical mandrels and incorporated longitudinal yarns to create a triaxial construction with a $0°/\pm\theta°$ orientation (Fig. 1). Four different braid geometries were manufactured [3]. The braid angle, the yarn sizes, and the longitudinal yarn content were varied to determine sensitivity to these parameters. The desired thickness was obtained by overbraiding layers. Since all specimens had the same nominal thickness of 6.35 mm, the number of layers decreased with increasing yarn bundle size.

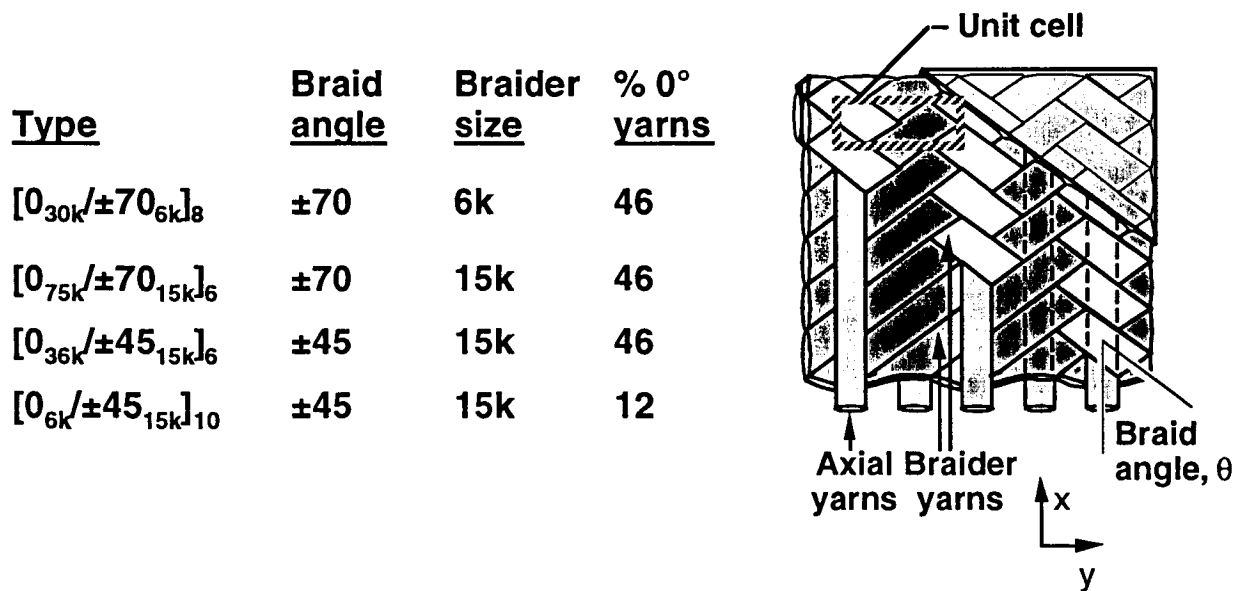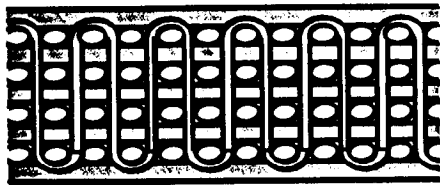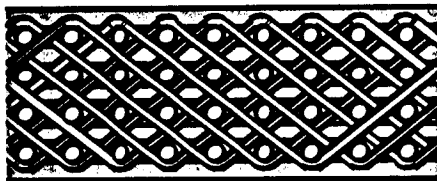| Type | Braid angle | Braider size | % 0° yarns |
|---|---|---|---|
| $[0_{30K}/\pm70_{6K}]_8$ | $\pm70$ | 6k | 46 |
| $[0_{75K}/\pm70_{15K}]_6$ | $\pm70$ | 15k | 46 |
| $[0_{36K}/\pm45_{15K}]_6$ | $\pm45$ | 15k | 46 |
| $[0_{6K}/\pm45_{15K}]_{10}$ | $\pm45$ | 15k | 12 |



Figure 1. 2D triaxial braid architecture

The 2D-woven fabrics included a plain weave and two 5-harness satin weaves. One of the 5-harness satin weaves was made with 3k tows (AW280-5H), and one was made with 6k tows (AW370-5H). The plain weave (AW193PW) was used to make two panels of 12 and 16 layers. The panels made from the satin weaves were 12 layers thick. The 3D weaves were all interlock woven fabrics where yarns are woven through the thickness to provide direct resistance to delamination. The interlock tows ran parallel to the warp (0°) yarns and wrapped around the weft (90°) yarns. Three different weave architectures were investigated: through-the-thickness orthogonal interlock (OS), through-the-thickness angle interlock (TS), and layer-to-layer angle interlock (LS). The weave architectures are shown schematically in Fig. 2. For each
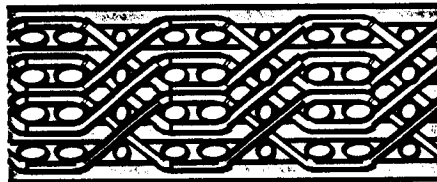
architecture, one panel was woven using small fiber bundles (-2), and one panel was woven using large fiber bundles (-1).



Through-the-thickness orthogonal interlock (OS)
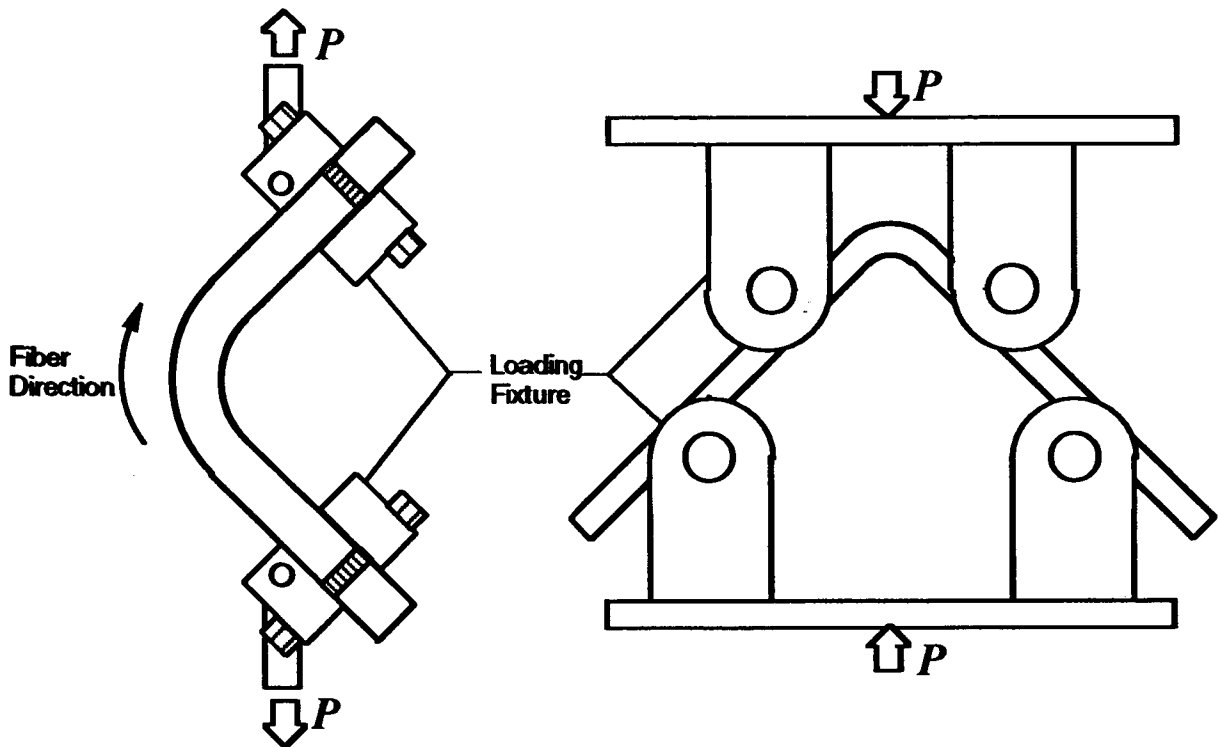
Through-the-thickness angle interlock (TS)

Layer-to-layer interlock (LS)

| Code | Warp # | size | Weft # | size | Weaver size |
|------|--------|------|--------|------|-------------|
| -1 | 4 | 24k | 5 | 12k | 6k |
| -2 | 6 | 12k | 7 | 6k | 3k |

Figure 2. 3D weave architecture

## Test Configuration and Data Reduction

Two different test configurations, shown schematically in Fig. 3, were used to measure strength. A new test method was evaluated which used a four-point-bending (4PB) fixture where the specimens were loaded by rollers to create a force couple on each loading arm [2]. Because of the geometry of the 4PB fixture, the specimens were self aligning. The second configuration used a steel hinged loading mechanism (HLM) which was aligned and clamped on to the specimen's loading arms [1]. This test method had been used previously to measure the strength of unidirectional laminates. This loading fixture allowed the specimen to be tested in a tension testing machine. The displacement was controlled at 0.2 in/min (0.5 mm/min) during loading for both test methods. Loads and displacements were digitally recorded. To aid in detecting failure location, the edges of each specimen were painted white with a water-based typewriter correction fluid.

Hinged Loading Mechanism       4-Point Bend Test Method
Test Method  (HLM)                    (4PB)

Figure 3.  Test configurations

The loads on the test section were calculated for both test configurations prior to analysis.  To calculate stresses in the curved segment, the applied loads had to be translated to the ends of the curved segment.  For the 4PB configuration, the applied moment on the curved section of the specimen is simply the product of the force exerted by one of the cylindrical loading bars and the distance between two bars along a loading arm (Fig. 4).  The bar force and distance were calculated from the total load and the geometries of the loading fixture and test specimen [2].  Since a force couple acts on the loading arm, the resultant force is zero.  For the HLM test configuration, a similar procedure was followed to calculate the loading [1].  The resultant force, however, is nonzero for this case (P ≠ 0).  These results are shown schematically in Figure 4.
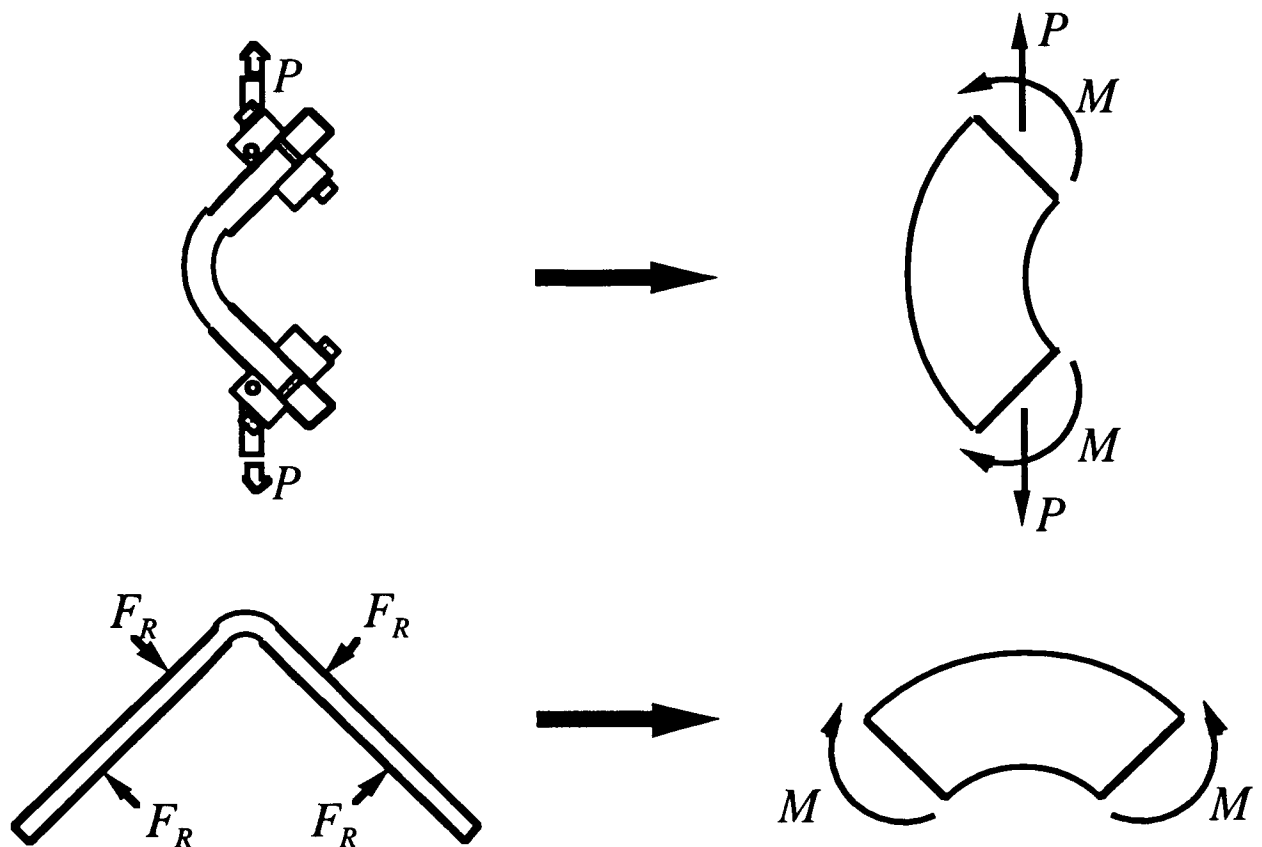
Figure 4. Translation of forces

Solutions were developed by Lekhnitskii for the stresses in a curved beam segment with cylindrical anisotropy [4]. Using the translated loads at the ends of the curved segment, the stresses were calculated using the Lekhnitskii stress equations. For the hinged test configuration, the stress equations become more complex since the stresses produced by the moment and the end force must be superimposed [1]. Also, because of the end force, the stresses become a function of angular position. However, in the four-point-bending test configuration, the curved segment is under a state of pure bending. Consequently, the closed-form stress analysis is much simpler and independent of angular position [2]. Nevertheless, the stress fields produced in the curved region are only slightly different for the two different loading methods. Typical radial and tangential stress distributions, $\sigma_r$ and $\sigma_\theta$, along the centerline of the specimen are shown in Figure 5. The radial stress, $\sigma_r$, reaches a maximum at approximately 35% of thickness from the inner radius and is zero at both free edges. The tangential stress, $\sigma_\theta$, ranges from tension on the inner radius to compression at the outer radius.
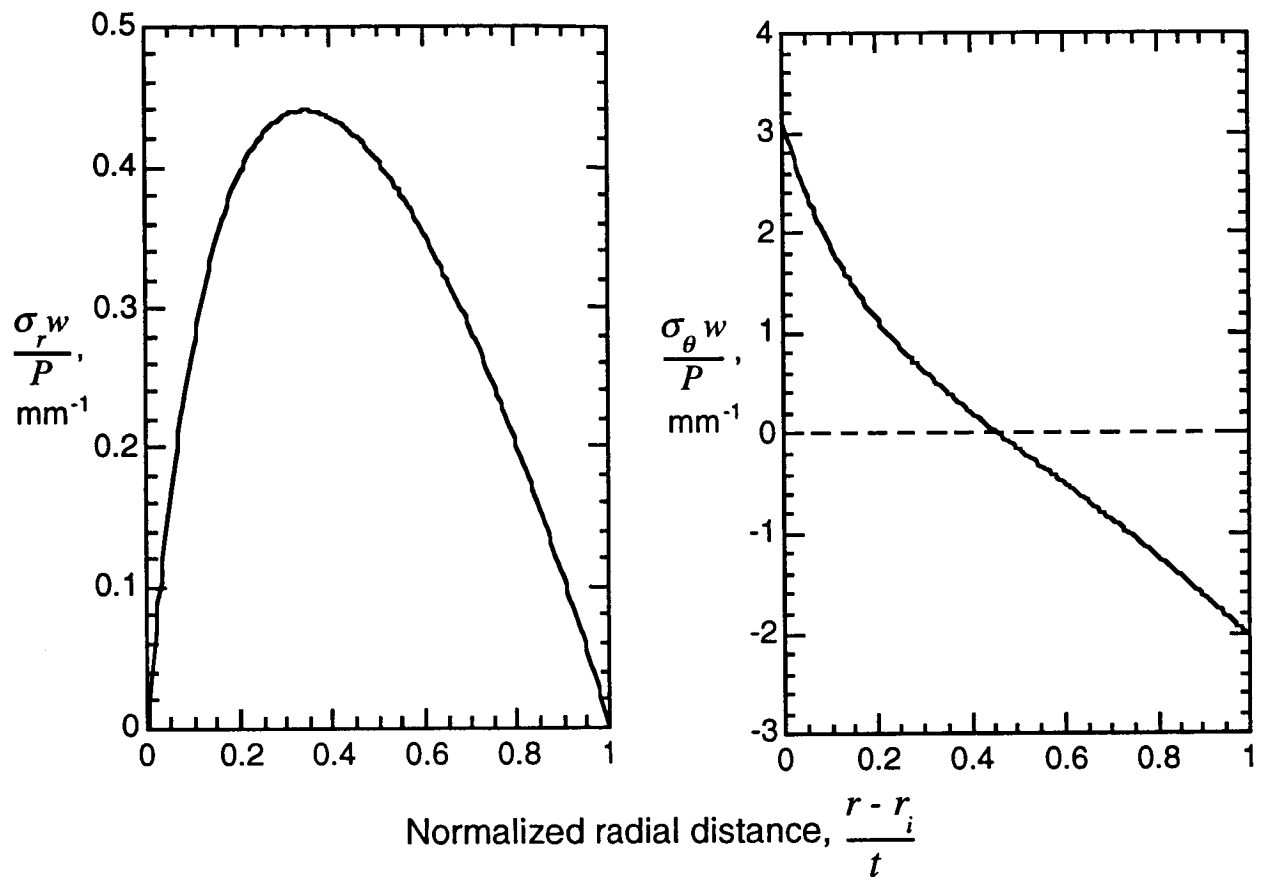
Figure 5. Typical stress distribution for a curved beam under bending

## Experimental    Results

Each specimen was loaded to failure using either the four-point-bending fixtui (4PB) or the hinged loading mechanism (HLM).  A typical load history to failure is shown in Figure 6 for a 48-ply AS4/8551-7 specimen using the 4PB fixture.  At failure the load drops sharply due to the stiffness loss caused by the unstable formation of circumferential  delaminations.
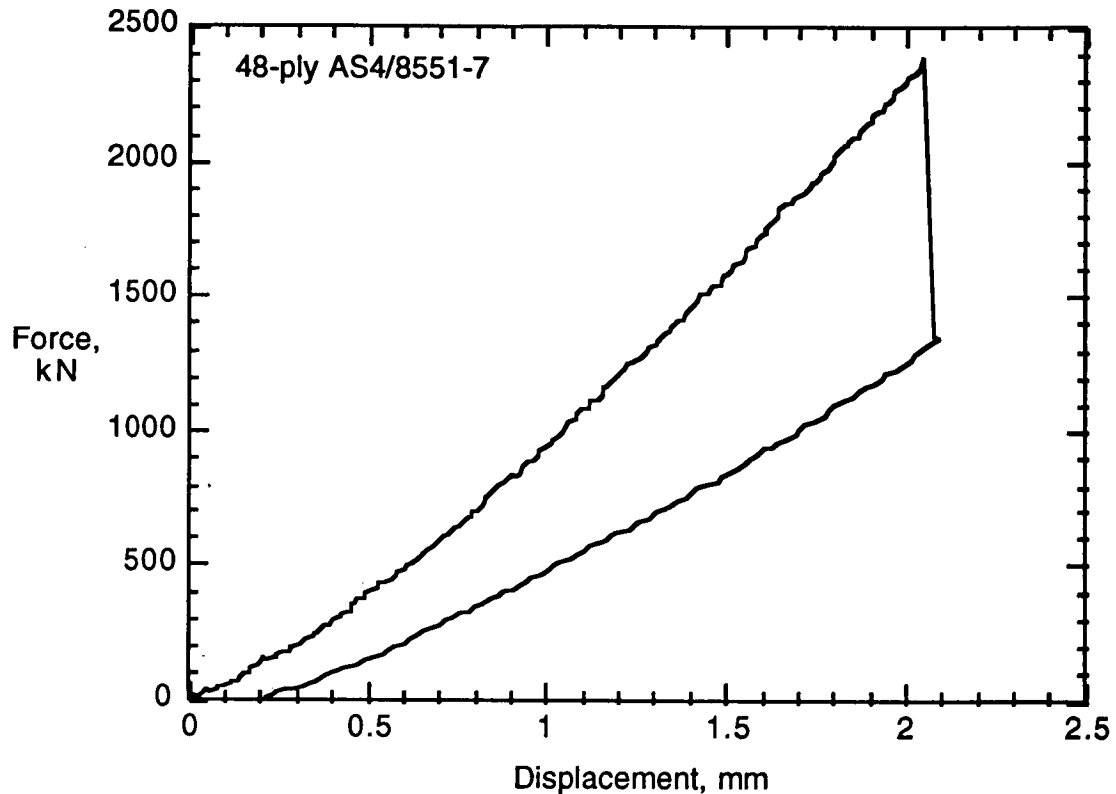


Figure 6.  Typical load history

Failures were significantly different between the 2D materials and the 3D weaves (Fig. 7).  Moiré fringe patterns provided an excellent method of detecting and documenting damage [1,5].  All the 2D materials (tapes, fabrics, and triaxial braids) simply delaminated between layers due to the out-of-plane tensile stresses.  No damage was detected prior to delamination.  Often, subsequent delaminations were also formed due to load redistribution into the sublaminates.  The delaminations in the 2-D braids often followed a tortuous path due to the nested layers.  In the 3D weaves, damage began accumulating very early in the loading.  During loading, the specimens emitted a crackling noise which was produced by radial cracks forming between the 90° (weft) surface plies in the inner radius caused by the tensile circumferential stress. Matrix cracking around the interlock tows was also observed.  The radial cracks

extended across the entire width of the specimen. Some of the radial cracks extended a third of the way into the thickness. Despite the through-the-thickness reinforcement, circumferential cracks similar to the 2D materials eventually formed. The OS-2 weave, however, never formed a circumferential crack. Since the cracks in the inner radius significantly alter the stresses in the bend, a through-the-thickness stress at failure could not be calculated for the 3D weaves.

# Failure Modes

## Layered Material (Tapes, 2-D Weaves, 2-D Braids)

## Non-Layered Material (3-D Weaves)

Figure 7. Typical failure modes

A summary of the average strengths (maximum $\sigma_r$ at the onset of damage) along with the high/low data is shown in Fig. 8 for all the 2D materials. In general, the 2D textile materials had very similar strengths with the range of strengths overlapping for each of the material systems. However, the through-the-thickness strength was generally lower than in the tape materials. The 48-ply AS4/3501-6 tape material had a similar strength to the 2D textiles but had a low fiber volume fraction. The through-the-thickness strengths of the specimens made from the prepreg materials, and possibly the RTM materials, decreased rapidly with decreasing fiber volume fraction.
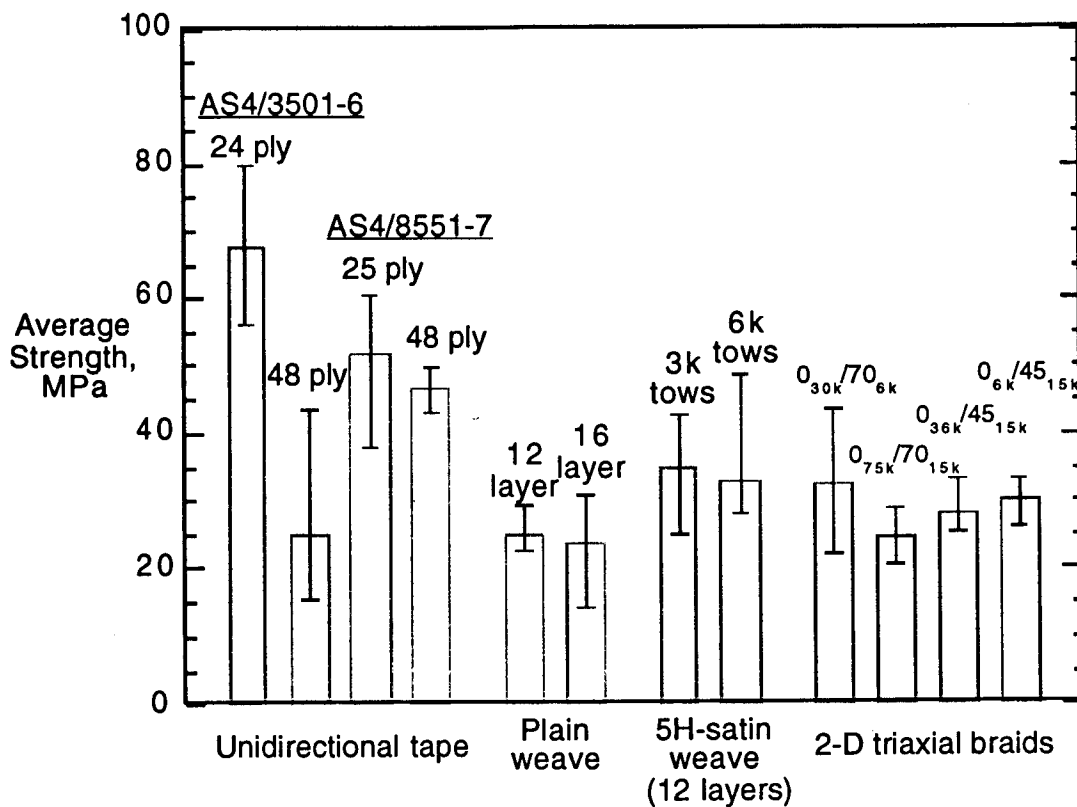


Figure 8. Average strengths of 2D materials

For the AS4/3501-6, the 24-ply strength was significantly higher than the 48-ply strength but had a much higher fiber volume fraction (Fig. 9). Excluding volumetric effects, the through-the-thickness strength should be independent of thickness. The average ply thickness in the bend was 0.165 mm in the 48-ply specimens and 0.133 mm in the 24-ply specimens. In previous tests, a strong correlation was found between ply thickness and strength. Therefore, the large strength difference may be a result of the 24% increase in ply thickness (decrease in fiber volume). The average

324

ply thicknesses of the 25 and 48-ply AS4/8551-7 specimens were nearly identical at 0.157 and 0.156 mm, respectively. Accordingly, the strengths were also close and within the scatter of data. The manufacturer's product data sheet for AS4/3501-6 lists a ply thickness of 0.13 mm to achieve a 62% fiber volume fraction. Since the AS4/3501-6 and AS4/8551-7 materials had identical fiber areal weights (149 g/m$^2$), identical ply thicknesses represent identical fiber volume fractions. Consequently, the strengths between the two material systems were only compared for similar fiber volume fractions. The average ply thicknesses of the 48-ply 3501-6 specimens and all the 8551-7 specimens were within 6%. For this case, the 8551-7 has nearly twice the strength of the 3501-6 material.
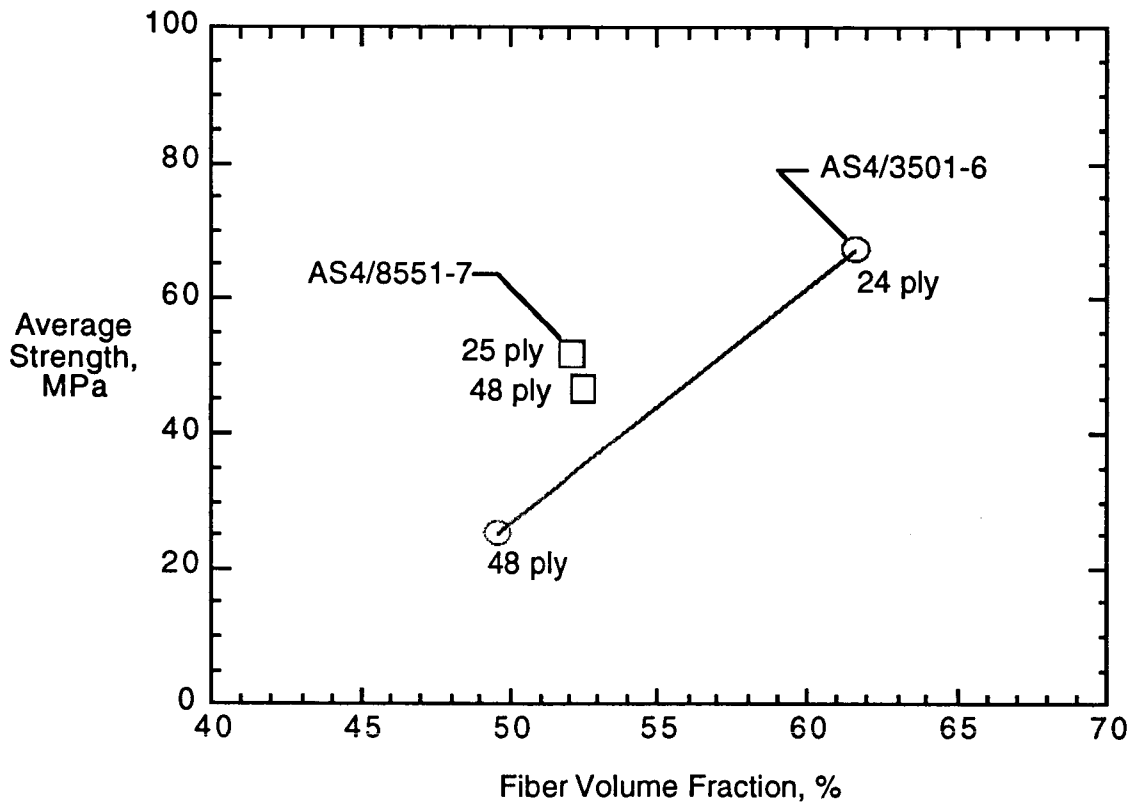


Figure 9. Effect of fiber volume fraction

The strengths of the 12- and 16-layer plain weaves were nearly identical. The average layer thickness in the bend was 0.208 mm for both thicknesses. The average layer thicknesses in the loading arms were 0.180 and 0.178-mm for the 12- and 16-layer specimens, respectively. The manufacturer's product data sheet lists a ply thickness of 0.18 mm for a 62% fiber volume fraction. Therefore, these strengths may increase with higher compaction. The two 5H-satin weaves also had nearly identical strengths. For the weave with 3k tows, the average layer thickness was 0.301 mm in the bend whereas the product data sheet lists a thickness of 0.25 mm for a 62% fiber

325

volume fraction. For the weave with 6k tows, the average layer thickness was 0.347 mm in the bend and the corresponding value on the data sheet was 0.34 mm for a 62% fiber volume fraction. Therefore, for equal fiber volume fractions, the 3k weave may have a higher strength.

Since stresses in a damaged material cannot be readily calculated, the moment at failure was calculated for the 3D weaves. The failure load was defined as the load where circumferential cracks formed. The circumferential cracks reduced the bending stiffness and caused a small drop in load. The average bending moment at failure is shown in Fig. 10 for tests using the 4PB fixture. Many of the 2D materials are also included for comparison. The OS-2 weave is not shown since circumferential cracks did not form. The bending moment was normalized by the width and thickness of each specimen for comparison. The 3D weaves all failed at significantly lower bending moments than all of the 2D materials. This 3D architecture failed at lower loads due to the radial cracking between the 90° (weft) surface plies along the inner radius. For the six 3D weave architectures, the bending moments at failure were all within 20% of each other. When analyzed in terms of the bending moment, the 2D materials had relative rankings nearly identical to the strength analysis.
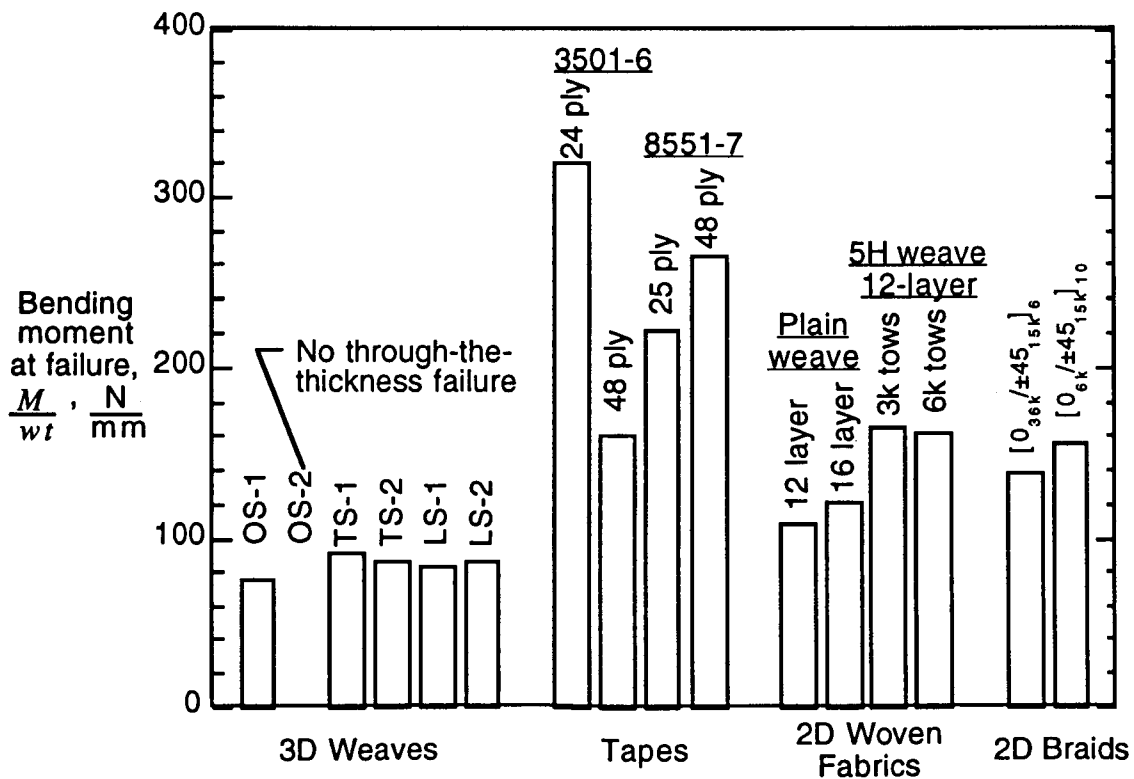


Figure 10. Average bending moment at failure

Specimens taken from the same panel were tested using both test methods to determine the effects on strength. A comparison of strengths measured using the two different test methods is shown in Fig. 11 for seven panels which represent all the 2D material types. The range of strengths, indicated by symbols, is also shown in the figure. For most of the materials, the average strengths were quite close considering the scatter in the data. Some differences may arise because of variations in specimen quality since specimens for each test method came from opposite sides of the same panel. Consequently, if the quality of the panel varied from side to side, a disparity in strengths would be exhibited between the two test methods. In the 16-layer plain weave panel, the two adjacent specimens that were tested using different test methods had identical strengths yet the overall averages differed by 24%. Also, less scatter was expected using the 4PB test since the specimens were self aligning while, in the HLM test, the hinges must be precisely positioned by hand. However, the scatter in the data was similar between the two methods.
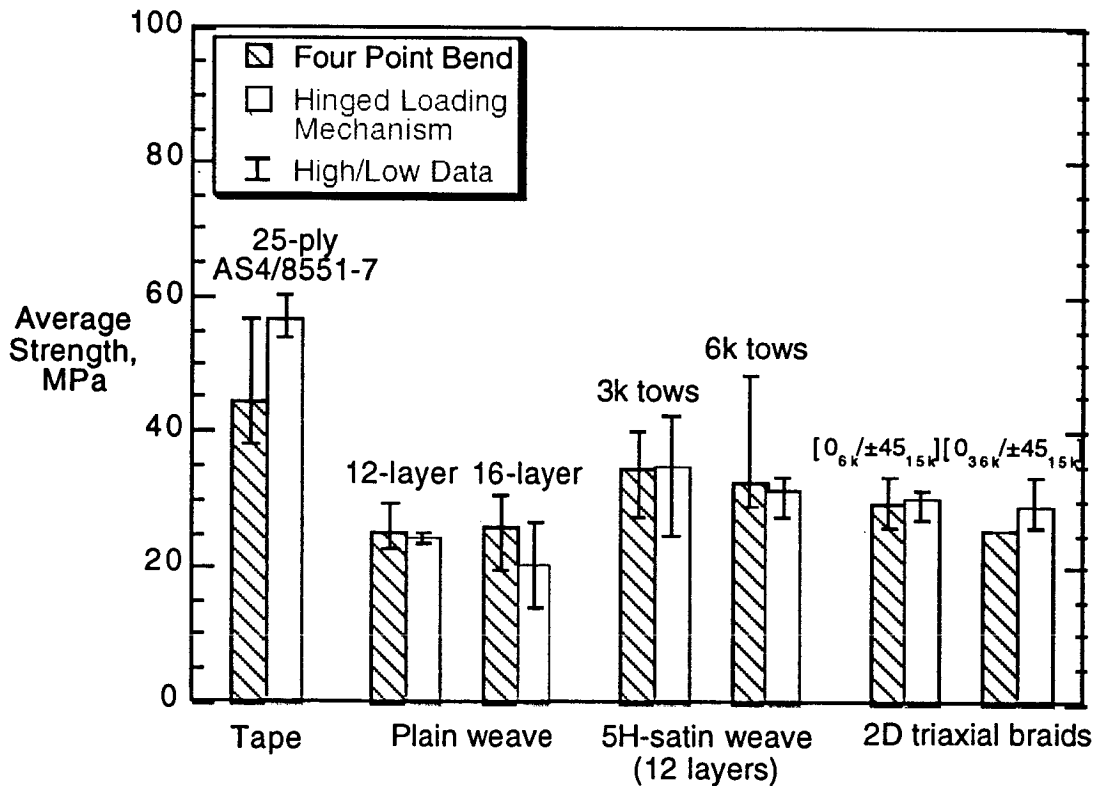


Figure 11. Comparison of strength data from the two test methods

## Summary - Through-the-Thickness Strength

Curved beams made from a variety of 2D and 3D composites were tested to determine the through-the-thickness strength. A new test configuration that used a four-point-bending fixture was evaluated and compared to a configuration that used a hinged loading mechanism. Both test methods produced identical failures at nearly identical stresses. However, the four-point-bend test method was the preferred test method since it was self-aligning and did not require laborious positioning and clamping of hinges onto the specimen. In addition, the strength analysis was greatly simplified since a constant moment was produced in the test section.

Failures were significantly different between the 2D materials and the 3D weaves. The 2D materials delaminated between layers due to out-of-plane tensile stresses. At failure, the sublaminates formed by the initial delamination would often delaminate to form more sublaminates. The delaminations between braided layers followed a more tortuous path than the other 2D materials. Initial damage in the 3D weaves occurred very early in the loading and was made up of a series of radial cracks caused by the tensile circumferential stress along the inner radius. Final failure was caused by the formation of circumferential cracks around the test section similar to the 2D materials. Circumferential cracks did not form in the OS-2 weave, however. Due to the radial cracks, a through-the-thickness strength could not be calculated for the 3D weaves.

The strength of the 2D textile composites was lower than the tapes. The through-the-thickness strength was found to decrease significantly with decreasing fiber volume fractions. Final failure in the 3D weaves occurred at a lower bending moment than the other materials. The early failures were caused by the formation of radial cracks due to bending rather than a lower through-the-thickness strength.

# Standard Impact Test Method Development

This investigation focused on the development of a standard impact test method to measure impact damage resistance. Existing impact test methods were first evaluated to determine their suitability. Since a suitable test was not found, a new test was developed to isolate damage resistance. Working through standards organization such as ASTM and Mil-Handbook 17, the new test method is being further developed and promoted for adoption. New research in this program is going to focus on the development of "rules" for damage tolerance testing.

### Existing Impact Test Methods

The only impact tests that currently exist are compression after impact (CAI) tests which incorporate elements of both damage resistance and damage tolerance. The only results typically reported from CAI tests are compression strengths. Since the compression strength is a function of both damage resistance and damage tolerance, the user is unable to determine which properties were improved or not improved. An improvement in CAI strength could even be caused by an improvement in damage

resistance but a decrease in damage tolerance. In addition, all CAI test results are based on impacter kinetic energy. Consequently, the amount of damage is a function of target and impacter configuration (i.e., plate size, BC's, indenter diameter, etc.) [6]. Several CAI test methods are commonly used which all have different target and impacter configurations (Boeing, SACMA, and NASA). Consequently, results from one test method cannot be compared with results from a different method. In addition, since the results are configuration dependent, the results from coupon test cannot be easily scaled to plate of different sizes and boundary conditions. A typical impact test method is shown in Figure 12.

# SACMA Recommended Impact Test Method

Specimen Size: 4 x 6 inches
Impact Energy: 1500 in-lb/inch thickness
Impacter Mass: 11 lbs recommended
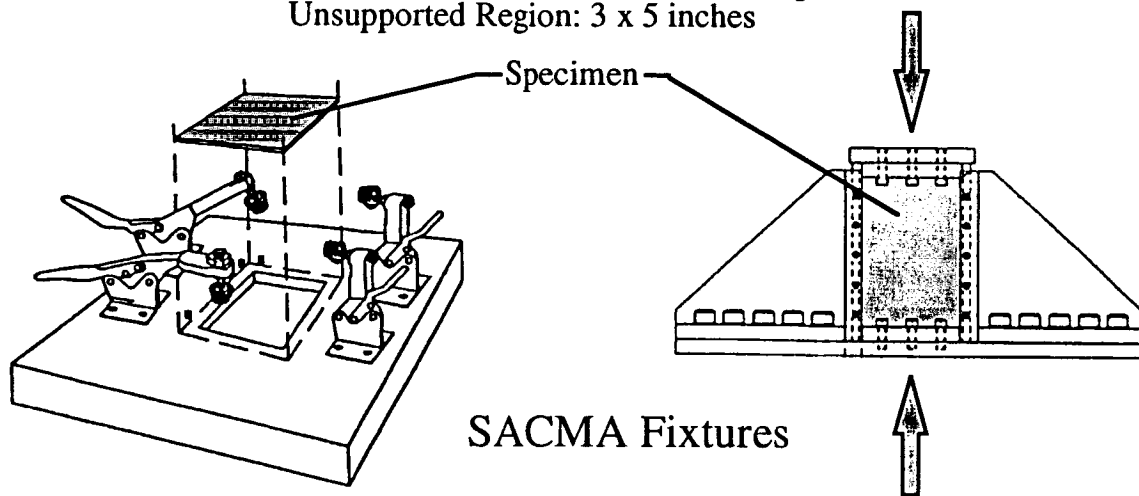Indenter: 0.625-inch diameter hemispherical
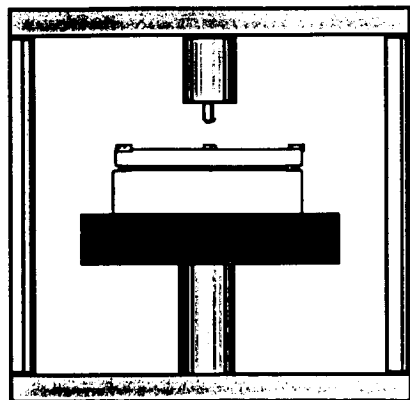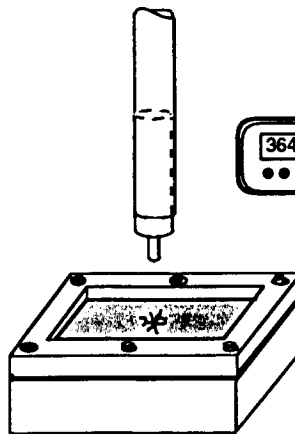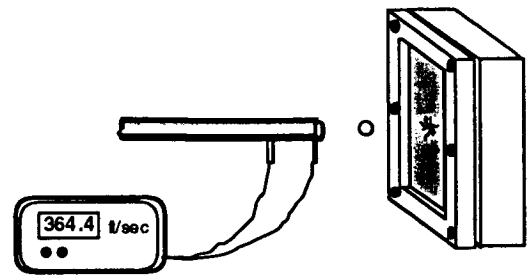Unsupported Region: 3 x 5 inches

Figure 12. Typical CAI impact test

Impact tests can be performed with a large range of impacter mass and velocity combinations. Depending on these combinations, the impact specimen can respond in various manners. Commonly used impact methods are shown in Figure 13. A quasi-static indentation (QSI) test uses a universal test stand to slowly apply a transverse load. A falling weight impact test typically uses a large mass dropped from relatively low heights. The air gun impact test uses a small mass projectile fired down a barrel. It has been shown for many cases that a relatively small plate impacted by a large mass will deform in a quasi-static manner [6-8].
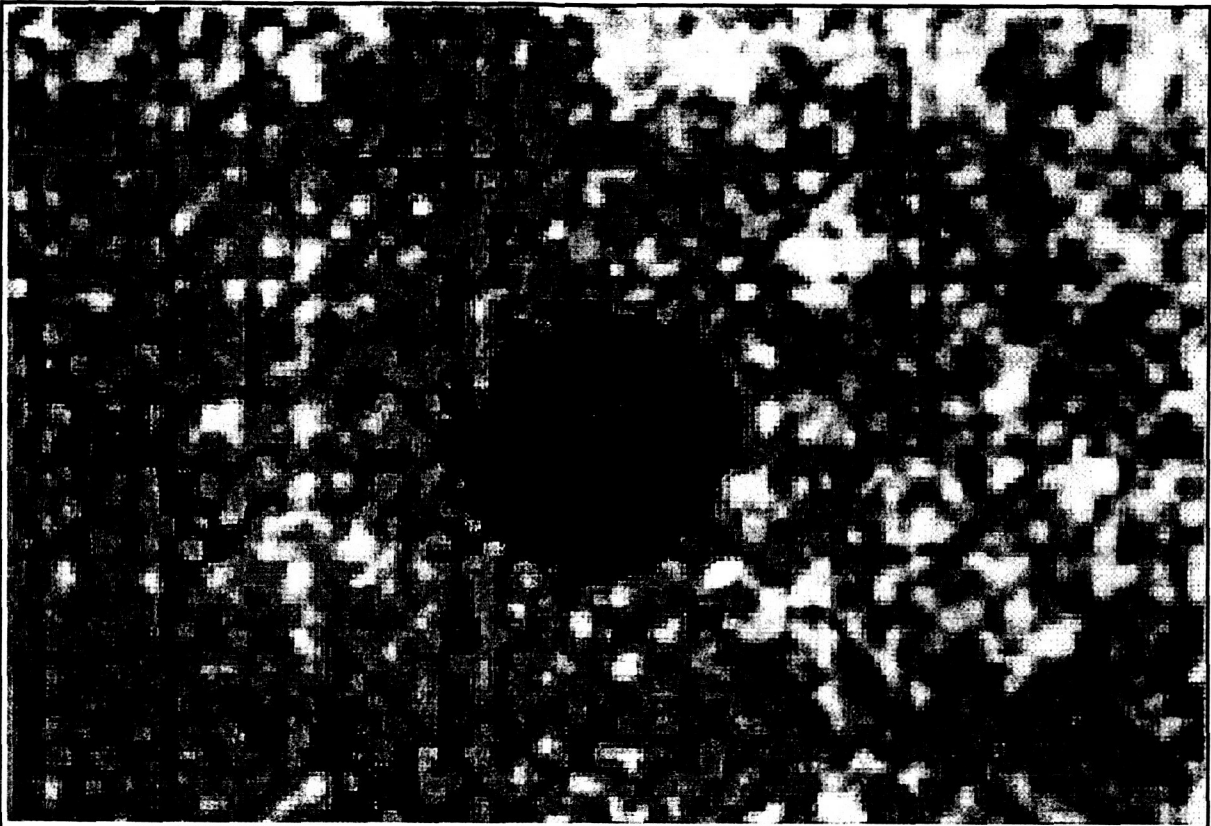
329

**Static Indentation**  **Falling Weight**  **Air Gun**

Figure 13. Impact methods

The quasi-static indentation (QSI) test was selected for development to measure damage resistance. This test method is the easiest of the three methods to use since it requires no special testing equipment. In addition, the force is applied very slowly under displacement control which allows for additional measurements during the test. Since a quasi-static deformation occurs, the test closely simulates the falling-weight impact test in many cases. By using impact force rather than impact energy, the damage is much less dependent on the impact configuration. Damage resistance is quantified in terms of the contact force to produce a unit of damage where the metric for damage may be damage diameter in C-scan, depth of residual dent, penetration, damage growth, etc. Some of these parameters (C-scan damage diameter and dent depth) are a function of the applied force. Consequently, the QSI tests must be done in increments if these parameters are to be monitored. A typical c-scan of impact damage in a 48-ply quasi-isotropic carbon/epoxy laminate is shown in Figure 14.

**AS4/3501-6 Quasi-Isotropic Laminate**

Figure 14. A typical c-scan of impact damage

A final draft of an impact standard that uses a QSI test method will be presented to the ASTM Impact Task Group (D30.02.06) at the May 1995 meeting. In this document, the impact test will be run quasi-statically under displacement control. A 6.0-inch-square specimen will be simply supported on a 5-inch-diameter ring. Many post-impact compression tests use a 4.0- x 6.0-inch square specimen. By using a 6.0-inch-square specimen, the edges can be trimmed to perform this damage tolerance test in an existing fixture. A 32-ply quasi-isotropic laminate has been specified for the impact specimen. The specimen will be indented using a 0.5-inch-hemispherical steel indenter. The force where damage first affects the force-displacement behavior (termed "$F_1$"), dent depth, and maximum force are specified to be recorded. The delamination size could not be included in this standard since ASTM does not currently have an NDE standard.

# Quasi-Static Indentation Tests on Textile Composite

To improve the weight saving benefits of carbon/epoxy materials, there is a need to improve the damage tolerance and delamination resistance of these materials. Composites made from textile materials may significantly improve these properties. In this investigation, the impact damage resistance behavior of a variety of textile materials was studied using the quasi-static indentation (QSI) test method. The force where large damage initiates was measured and the delamination size as a function of force was determined. The delamination diameter - impact force relationship was quantified using a damage resistance parameter, $Q^*$, which related delamination diameter to impact force over a range of delamination sizes.

## Test Procedure

The QSI tests were performed in a servo-hydraulic load frame under stroke control at a ramp rate of 0.02 in/min. All specimens were clamped firmly in an aluminum test fixture during testing. An instrumented tup attached to a 0.5-in-diameter hemispherical indenter was used to measure load. The tup was mounted in the grips of the load frame such that the indenter traveled normal relative to the face of the specimen. The indentation load and stroke output were recorded at a rate of one data point per second throughout the loading history using a digital data storage oscilloscope. The relevant damage and test parameters were measured and recorded after each test. Many of the test coupons were indented more than one time. Initially, each specimen was loaded to a pre-determined force and then unloaded. The damage and test parameters were then measured and recorded. After this initial series of measurements was taken, the specimen was then reloaded to a higher force and the series of measurements was repeated. This process was repeated at approximately 2.22 kN (500 lbf) increments until the delaminations had grown close to the edge of the test fixture.

## Materials

As in the through-the-thickness strength testing, a variety of textile and prepreg tape materials were used in this investigation. The same 2D triaxial braids (four different braid geometries), 3D interlock weaves (three architectures), and prepreg tape materials (AS4/3501-6 and AS4/8551-7) were used as in the previous investigation. Tape equivalents of the $[0_{6k}/\pm45_{15k}]$ triaxial braid and the TS-2 through-the-thickness angle interlock weave were also made from AS4/3501-6 for comparison purposes.

In addition to these materials, stitched and nonstitched uniwoven composite materials were evaluated. Stitched laminates were not used in the through-the-thickness testing since tightly curved stitched panels could not be manufactured. Four laminate thicknesses were manufactured with quasi-isotropic lay-ups of $[45°/0°/-45/90°]_{nx}$ where n = 2, 3, 4, and 6. These laminates were made from layers of dry uniweave carbon fabric which consisted of 97% Hercules AS4 carbon fibers and 3% fiberglass fill yarn by weight. The fill yarns were 225-denier fiberglass and were

woven normal to the carbon tows to hold the fibers together while stitching. The preforms for the stitched laminates were lock stitched at 8 penetrations per inch with a 1250 yd/lb fiberglass yarn. All stitching was in the 0° direction with 1/8-inch row spacing. The preforms were impregnated with Hercules 3501-6 epoxy by Douglas Aircraft Company using the resin transfer molding (RTM) process. After manufacture, all laminates were ultrasonically c-scanned to ensure that the panels were of high quality and free from manufacturing defects.

## Initial Delamination Growth

To gain a better understanding of the impact damage mechanics, particular damage events were related to the impact force where the event occurred. The force ($F_1$) where large damage initiates is one measure of impact damage resistance. This force was defined as the force at which the contact force versus indenter displacement curve changes because of damage formation or growth. At this force, a sharp load drop often occurs which is associated with unstable delamination growth. This unstable delamination growth typically causes a sudden loss of transverse stiffness and an audible "pop." The unstable delamination growth was used because of its ease of identification. Some matrix cracks and small delaminations may form just prior to the $F_1$ force. A comparison of $F_1$ forces for all of the materials was made.

### Stitched and Nonstitched Uniweaves
Each of these coupons was 4.00-in. square and contained in a fixture with a 3.00-in. square opening. The force - indenter displacement is shown for 16-ply stitched and nonstitched uniweaves in Figure 15. The stitched laminates could not be compacted to the same thickness as the nonstitched laminates. Consequently, the stitched laminates were slightly stiffer because of this increased thickness. The value of $F_1$ was approximately 10% higher in the stitched laminates than in the nonstitched. This slightly larger value of $F_1$ was attributed to the greater thickness of the stitched panels. For these thin specimens, a sharp load drop did not occur at $F_1$.
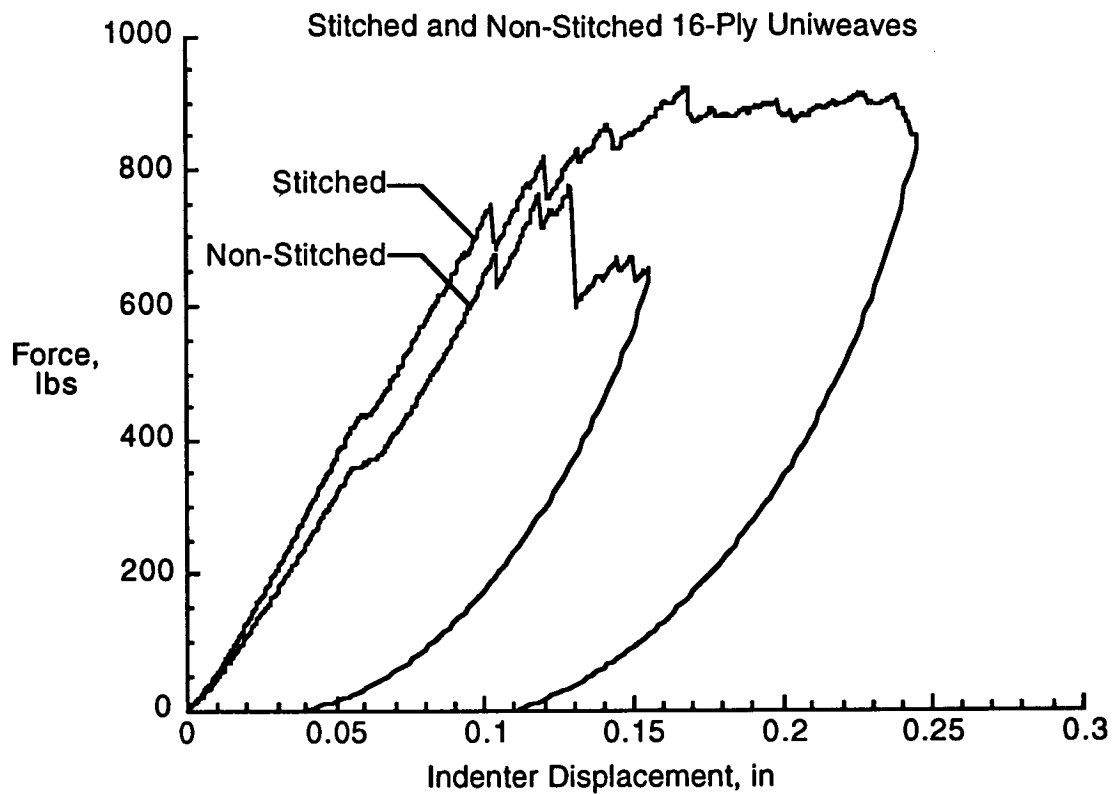
Figure 15. Quasi-static indentation of 16-ply stitched and non-stitched uniweaves

A similar plot of the force - indenter displacement is shown in Figure 16 for the 48-ply stitched and non-stitched laminates. Both of these laminates have similar transverse stiffnesses. The value of $F_1$ is approximately 20% lower for the stitched case. The nonstitched laminate has a sharp load drop at $F_1$ associated with unstable delamination growth. Stitching, however, appears to prevent this initial unstable delamination growth.



Figure 16. Quasi-static indentation of 48-ply stitched and non-stitched uniweaves

A summary of the average values of $F_1$ for the four different thicknesses of stitched and nonstitched laminates is shown in Figure 17. The initiation force decreased with decreasing plate thickness. For the 16-, 24-, and 32-ply laminates, stitching did not affect the value of $F_1$ by more than 10 %. However, for the 48-ply laminates, the value of $F_1$ was approximately 17% lower for the stitched laminates.
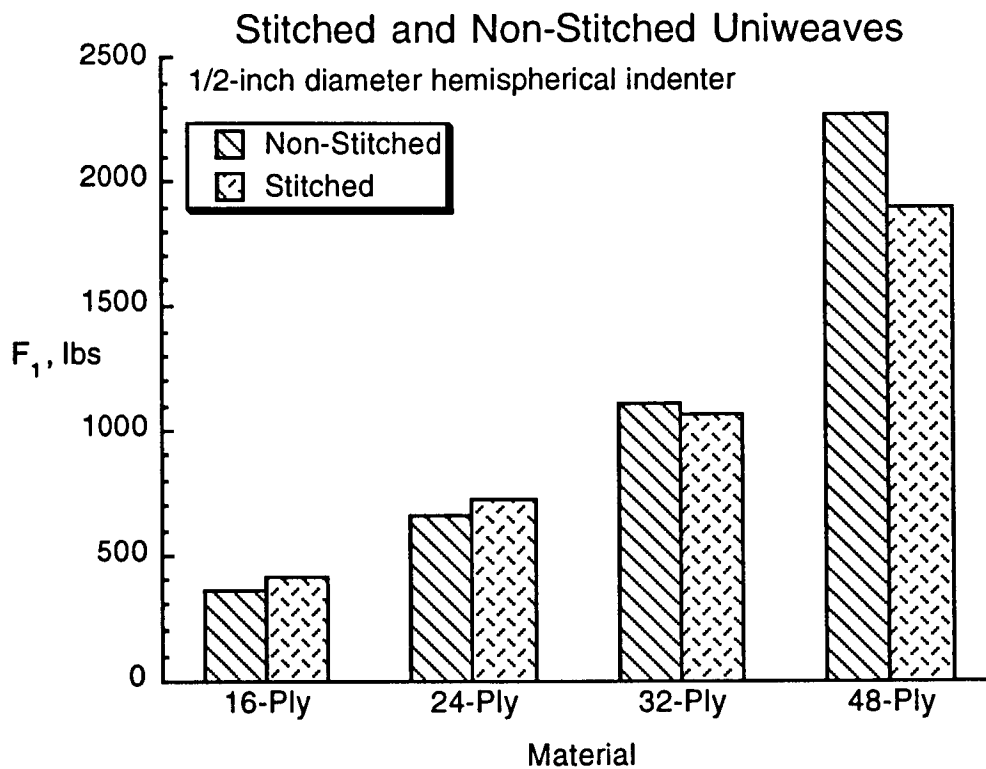


Figure 17. Average values of $F_1$ for stitched and non-stitched laminates

## 2D Triaxial Braids

Each of these coupons was 3.00-in. square and contained in a fixture with a 2.00-in. square opening. A smaller specimen had to be used due to a shortage of material. Previous studies have shown that the value of $F_1$ was independent of plate size. The force - indenter displacement is shown for three braids and a tape equivalent braid in Figure 18. The differences in stiffness between the different braids reflect the different fiber architectures which result in different flexural properties. All the braided panels were cured to the same thickness. The value of $F_1$ was easily identifiable since the layers of braided preform delaminate similarly to tape composites. However, there was no sharp drop in force when $F_1$ was reached. The tape equivalent laminate had a sharp load drop similar to the quasi-isotropic tape laminates.
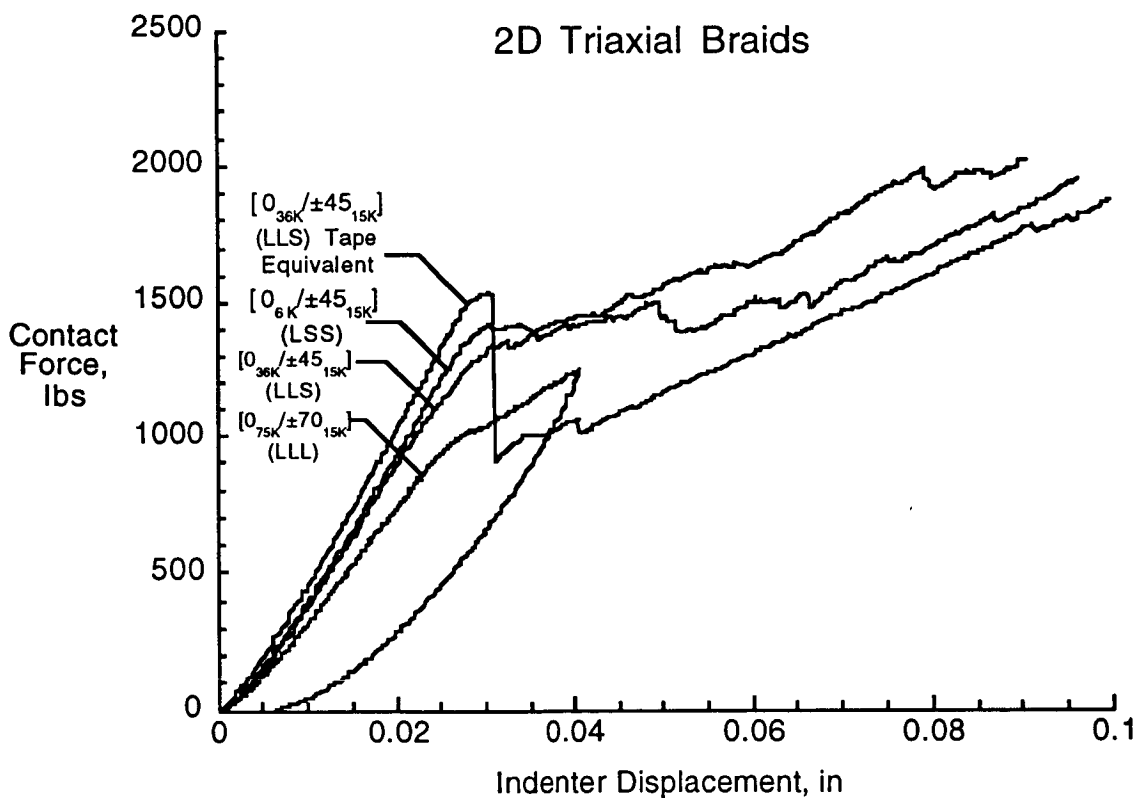


Figure 18. Quasi-static indentation of 2D triaxial braids.

337

A summary of the average values of $F_1$ for the 2D triaxial braids and a tape equivalent is shown in Figure 19. The $[0_{75K}/\pm70_{15K}]$ (LLL) braid had a lower value of $F_1$ (lower by a minimum 17% in all cases) than the other three braids. This lower value may be caused by the large 75k fixed yarns. The tape equivalent laminates had an average $F_1$ that was more than 25% greater than the actual braid.
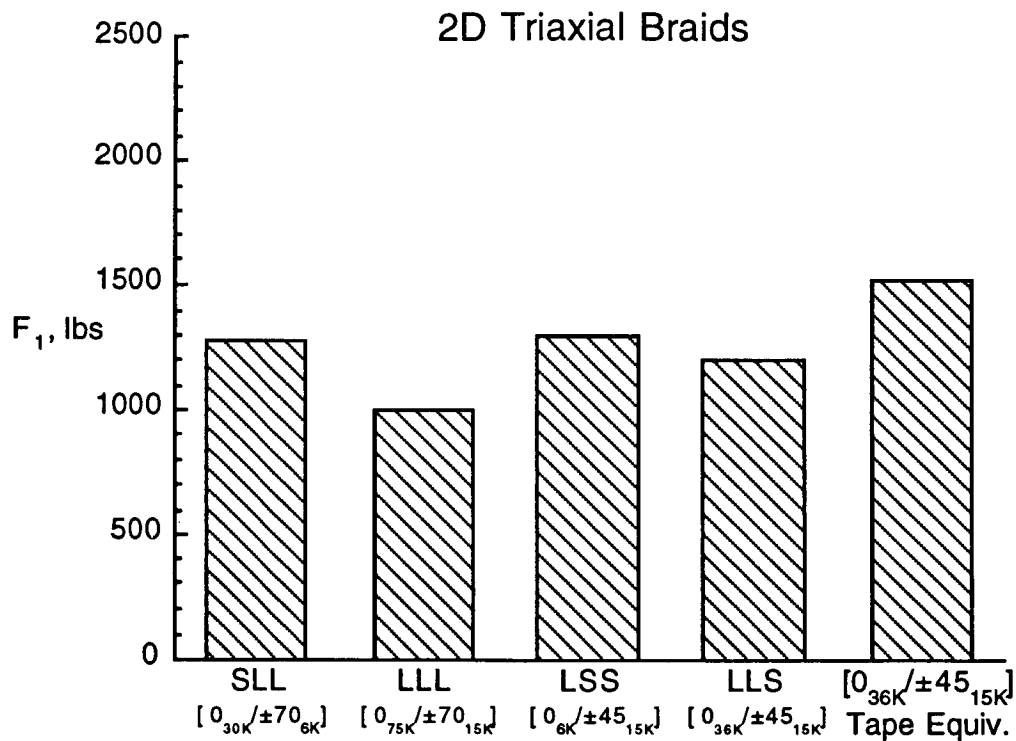


Figure 19. Average values of $F_1$ for 2D triaxial braids.

$Cl-2$.

## 3D Interlock Weaves

Again, small 3.00-in. square coupons contained in a fixture with a 2.00-in. square opening were used due to a shortage of material. The loading history is shown for three of the weaves and a tape equivalent weave in Figure 20. All woven panels were cured to the same thickness and, consequently, the differences in stiffness reflect the different textile architectures. The value of $F_1$ was not easily identifiable in several of the weaves. In the OS-2 weave, this point could not be identified at all since the material gradually lost stiffness. The OS-2 weave is also the only weave that did not delaminate in the through-the-thickness strength testing. Only the tape equivalent laminates showed a sharp drop in force when $F_1$ was reached.
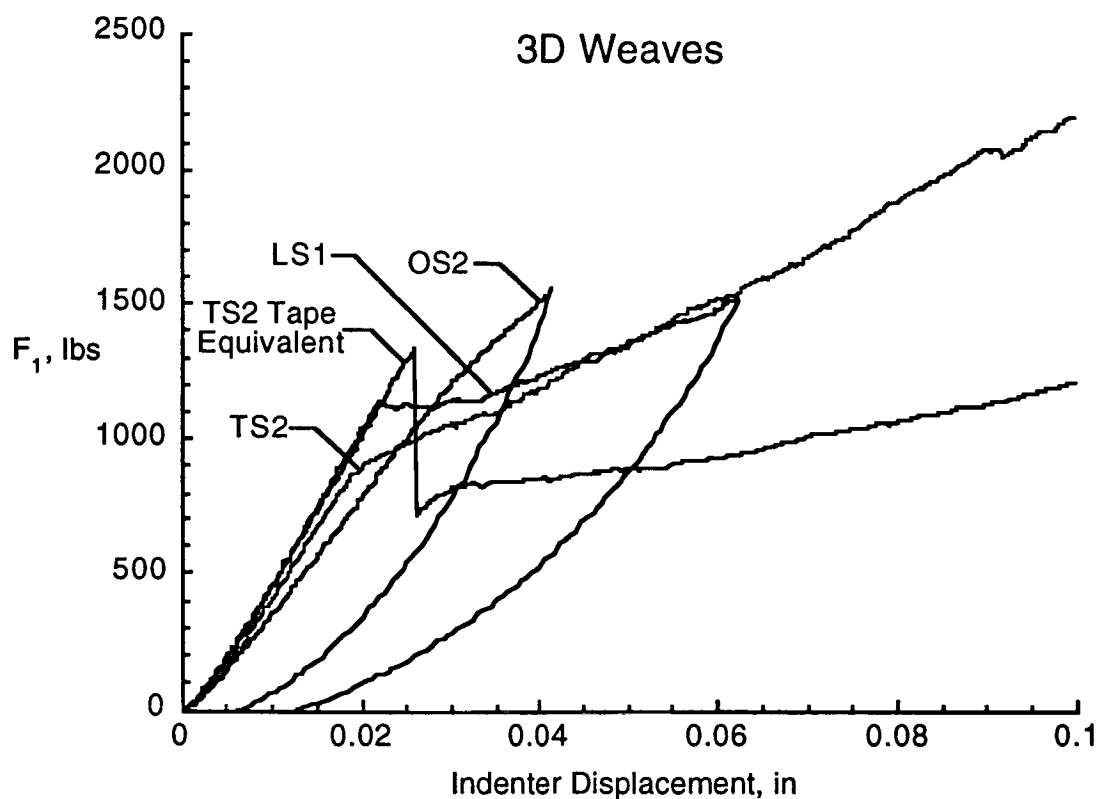


Figure 20. Quasi-static indentation of 3D weaves.

A summary of the average values of $F_1$ for the 3D weaves and a tape equivalent is shown in Figure 19. The LS and TS weaves have very similar values of $F_1$. The OS-1 weave has a slightly lower value of $F_1$ than the other weaves. Again, a distinct value of $F_1$ could not be identified for the OS-2 weaves. The TS-2 tape equivalent laminate had a 35% larger value of $F_1$ than the actual weave. The tow size did not affect the $F_1$ values for the LS and TS weaves. However, the smaller tows in the OS weave may have significantly reduced delaminations.
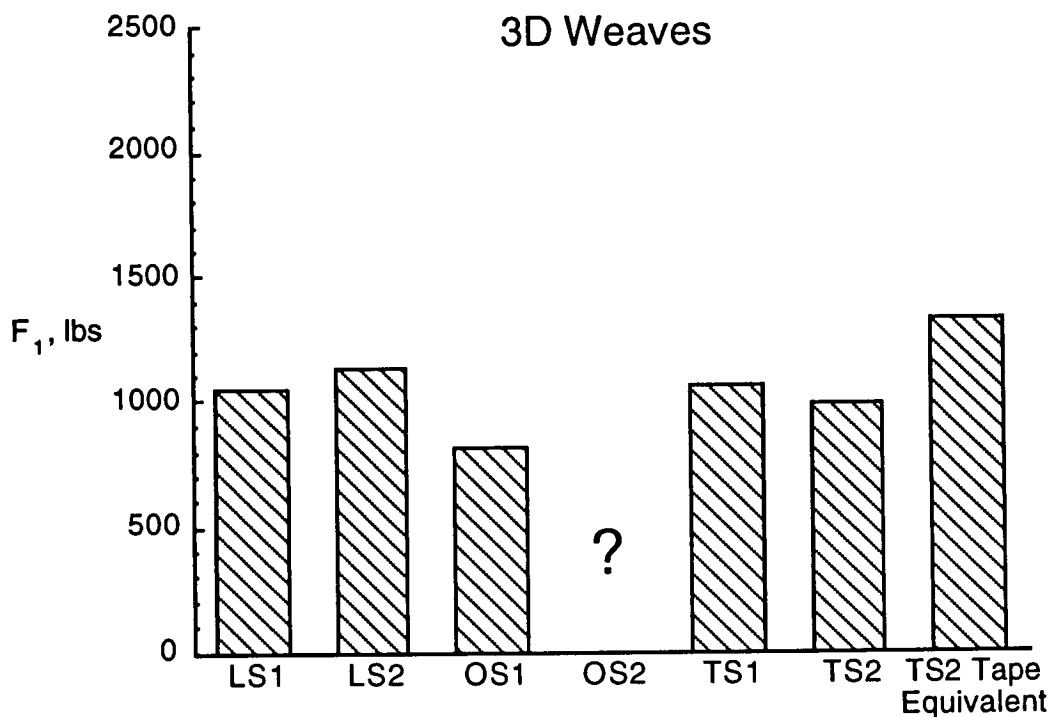


Figure 21. Average values of $F_1$ for 3D weaves.

An overall comparison of average $F_1$ values is shown in Figure 22 for all the different material systems. All of the comparison materials have a nominal thickness of 0.25 inches. In general, the tape materials performed significantly better than the weaves and the braids. The toughened tape (8551-7) had much higher values of $F_1$ than the non-toughened tape (3501-6). Stitching lowered the $F_1$ value relative to the nonstitched material. The tape equivalent laminates had lower values of $F_1$ than the quasi-isotropic tape laminates because multiple layers of tape were stacked on top of one another in the same orientation to simulate the thick layers of the braids and weaves.
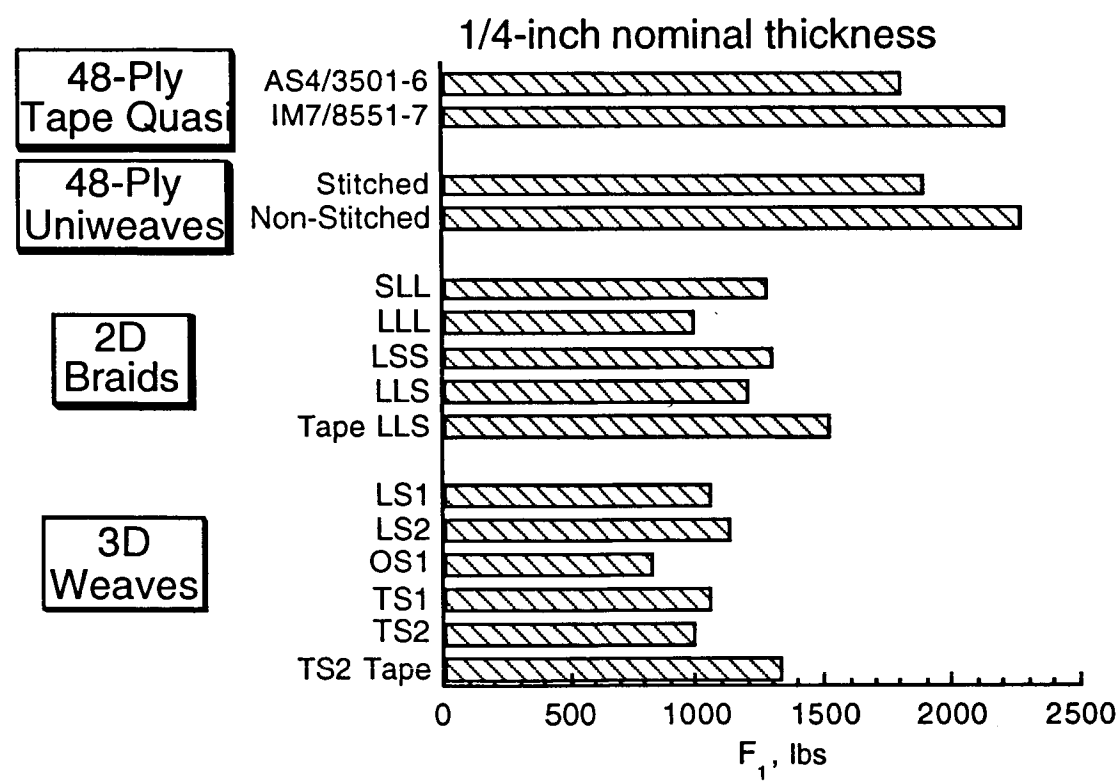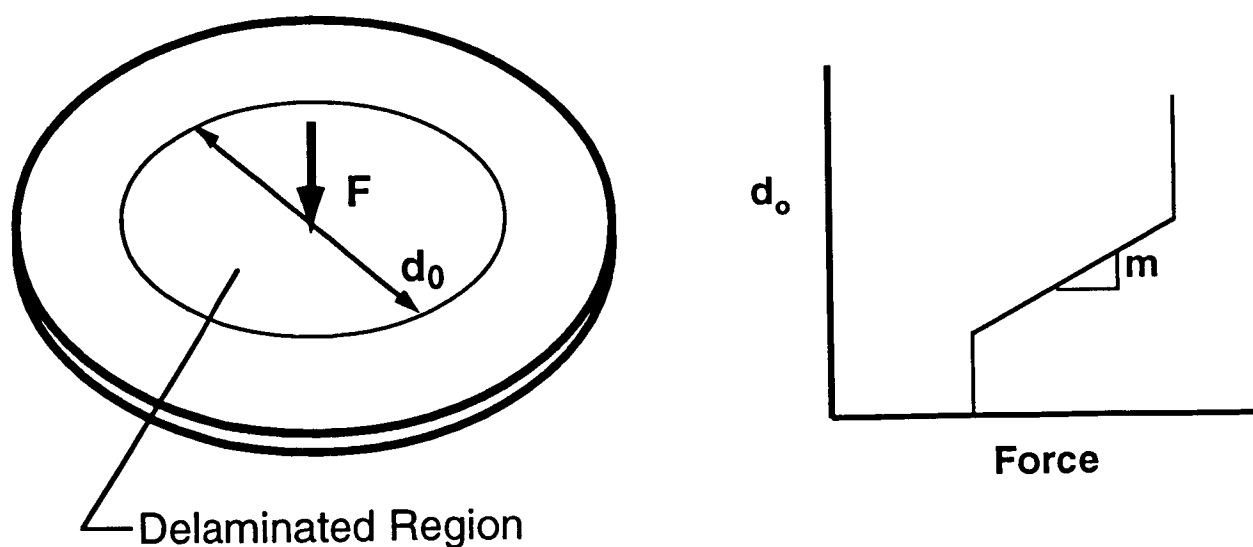


Figure 22. Overall comparison of average $F_1$ values for all material forms.

## Q* Damage Resistance Parameter

One objective of this study was to measure the damage resistance of different material forms over a range of damage sizes. CAI tests are generally performed at a single impact energy representing a single damage size. To quantify damage resistance over a range of damage sizes, a new method was used that relates damage size to impact force. In this method [6], a single damage resistance parameter called "Q*" provides a means to quantitatively rank the damage resistance. The analysis used to develop Q* was based on experimental observations involving impacts of quasi-isotropic plates. The Q* parameter represents the average transverse shear force per unit length associated with the edge of the delamination (Fig. 23). This parameter was observed to be constant between initial delamination growth and indenter penetration for quasi-isotropic laminated composites. By making Q* calculations, each materials ability to resist damage development or growth can be assessed.

To calculate Q*, the relationship between impact force and maximum delamination diameter, $d_0$, was determined. Q* is then calculated from the slope of the force - delamination diameter line between delamination initiation and indenter penetration (Fig. 23). The extent of the delamination was determined ultrasonically using c-scans. A c-scan provides a projection of all the various regions of delamination. The delamination area was calculated using image analysis and converted to diameter assuming a circular delamination area.



Delaminated Region

**From equilibrium:**

$$Q_r^* = \frac{F}{\pi d_0}$$

$$Q_r^* = \frac{1}{\pi m}$$

Figure 23. Calculation of the Q* damage resistance parameter.

An example of an impact force - delamination diameter plot is shown in Figure 24 for a 48-ply AS4/3501-6 quasi-isotropic laminate. A Q* of 75.0 kN/m was calculated from the slope of the line. There were no significant effects on the delamination diameter between running single tests per specimen versus multiple tests per specimen.
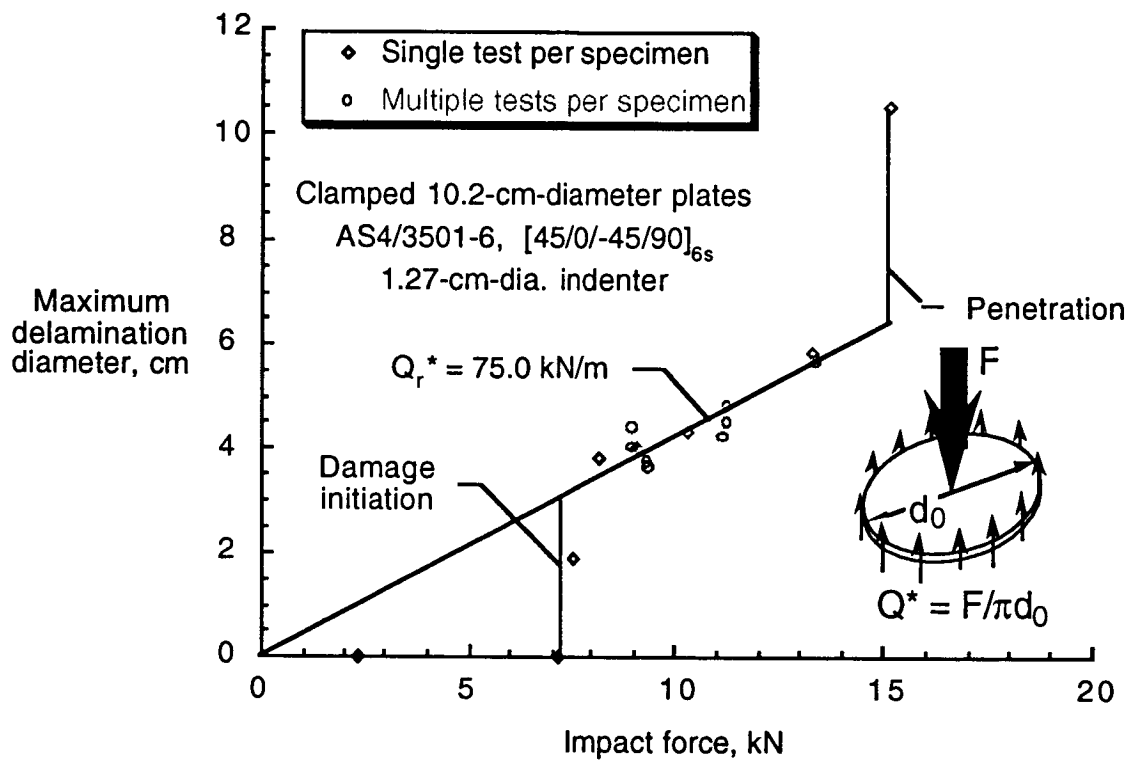


Figure 24. Delamination diameter as a function of impact force for AS4/3501-6.

The results of the Q* calculations for the stitched and nonstitched uniweaves are shown in Figure 25. Stitching increased the damage resistance as measured by Q* in all cases. The value of Q* increased with increasing plate thickness. For each material thickness, the improvement in Q* due to stitching also increased with plate thickness. The 48-ply plates showed the greatest improvements with a 90% increase in the Q* value while the 16-ply materials showed only a 23% increase.
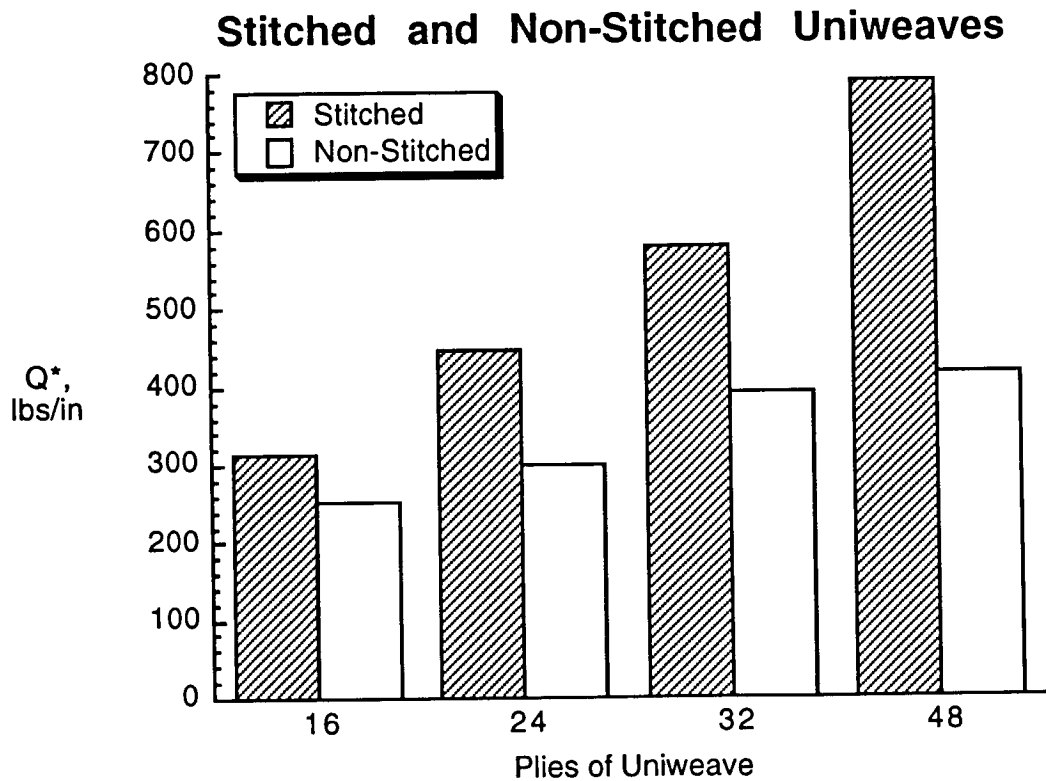
## Stitched and Non-Stitched Uniweaves



Figure 25. Comparison of Q* for stitched and nonstitched uniweaves.

In Figure 26, the results of the Q* calculations for the 2D triaxial braids are shown. All the braids except the LLL braid have Q* values within 1% of one another. The Q* value of the LLL was approximately 25% lower than the other braids. The nesting of the braided layers may have increased the damage resistance since the LLS tape equivalent laminate had a 22% lower value of Q* than the actual LLS braid.
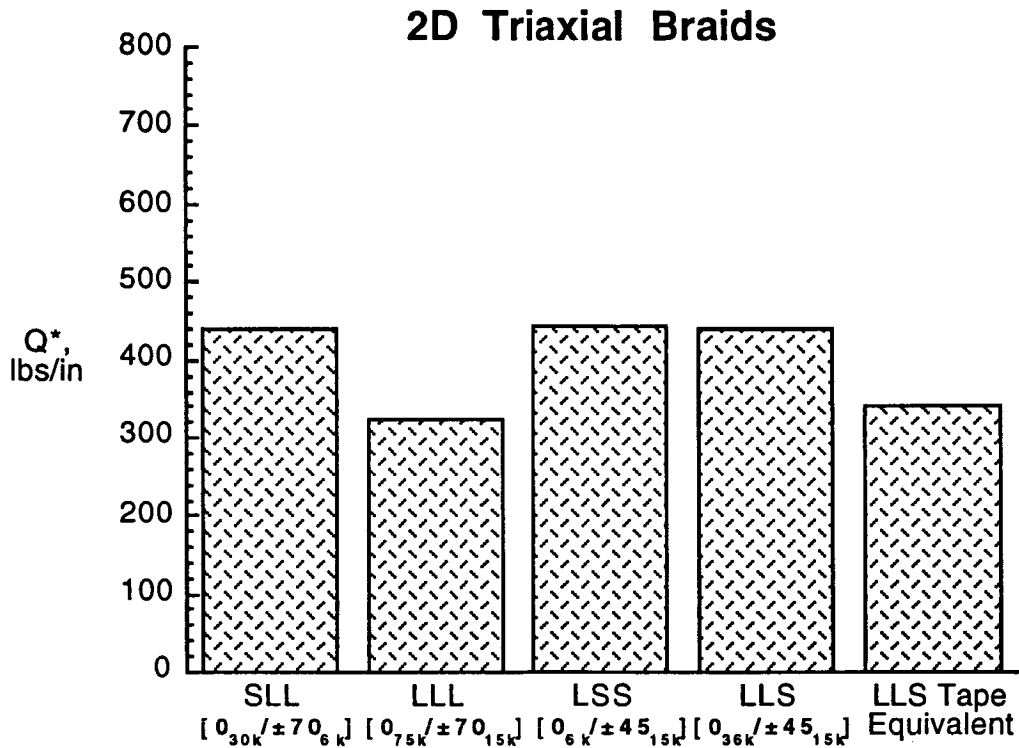


Figure 26. Comparison of Q* for 2D triaxial braids.

In Figure 27, the results of the Q* calculations for the 3D weaves and a ta[ equivalent weave are shown. In the LS and TS weaves, there was no significant effe on Q* as a result of using the smaller tows. However, in the OS weave, Q* increas( by more than a factor of two as a result of using the smaller tows. The OS-1 wea\ (larger tows) had Q* values comparable to the other weaves. The LS weave h\ approximately 25% lower values of Q* than the TS weave. The TS2 tape equivale laminate performed worse than the TS2 weave by about 50% showing that th through-the-thickness reinforcement was effective relative to a non-reinforce laminate.
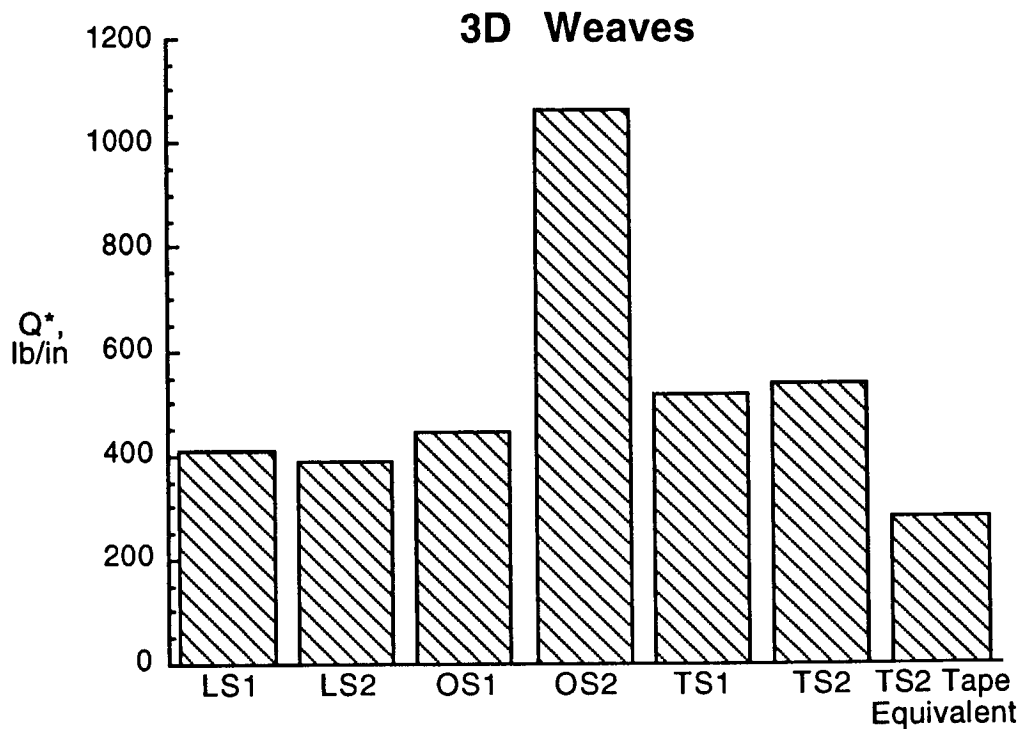


Figure 27. Comparison of Q* for 3D weaves.

An overall comparison is made in Figure 28 for all the 1/4-inch nominal thickness materials. The best performing materials were the toughened tape (IM7/8551-7), the stitched uniweave, and the OS-2 through-the-thickness orthogonal interlock weave. The delamination resistance of the braids (excluding the LLL braid) and the weaves (excluding the OS2 weave) was very similar to the quasi-isotropic tape (AS4/3501-6) and nonstitched uniweave laminates. The tape equivalent laminates and the LLL braid were the least resistant to delamination.
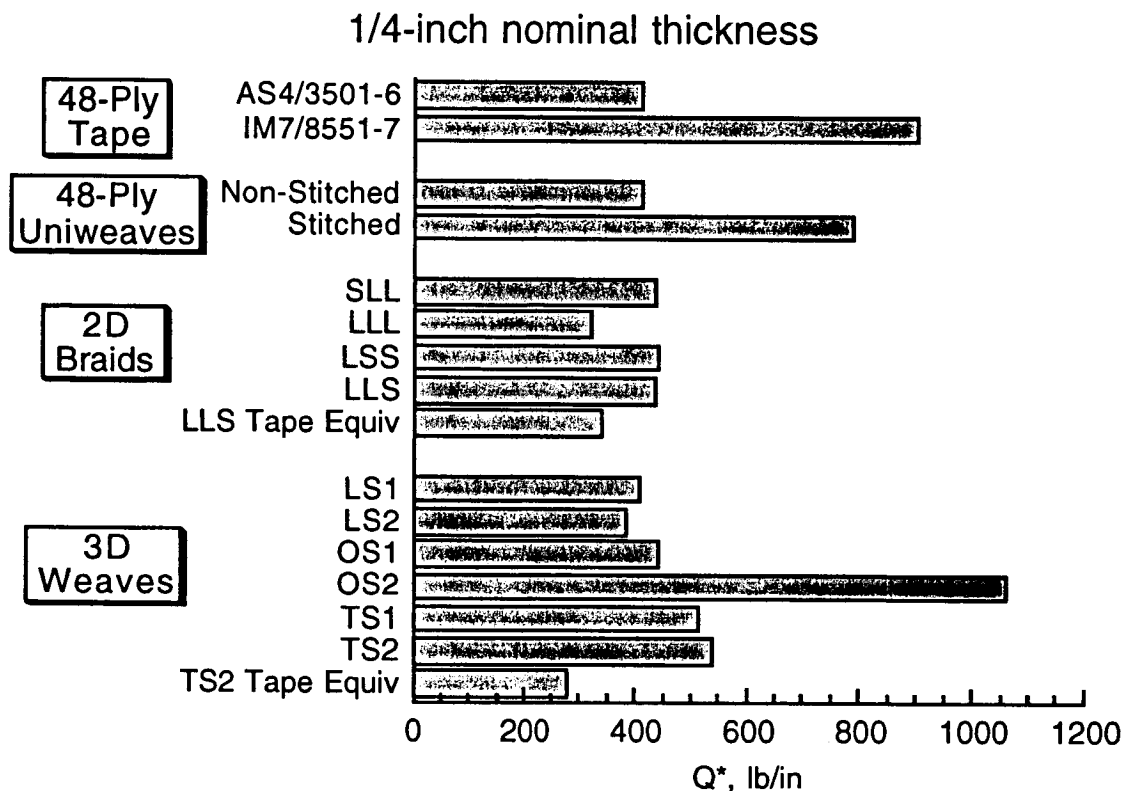
## 1/4-inch nominal thickness



Figure 28. Overall comparison of Q* for all materials.

## Summary - Quasi-Static Indentation Tests on Textile Composite

In braided and woven textile composites, the force to initiate delaminations ($F_1$) was significantly lower than in the tape or uniweave materials. The lower initiation forces may be due to the thicker layers used in these materials. Similarly, the tape equivalent laminates which had plies of the same direction grouped together also had lower values of $F_1$ relative to the 48-ply quasi-isotropic materials. Likewise, the LLL braid which had large 75k axial yarns had the lowest values of $F_1$. The equivalent laminates, however, had a higher value of $F_1$ than the textile which may indicate that fiber waviness also plays a roll in the low values of $F_1$. Except in the 48-ply laminates, stitching did not significantly affect the value of $F_1$. The damage resistance of these

347

materials, however, was significantly improved by stitching (smaller damage size for a given force). In general, the thicker plates showed the greatest improvements in damage resistance ($Q^*$) due to stitching.

The OS-2 weave was the only material where a distinct value of $F_1$ could not be determined. This material also had the best performance in terms of $Q^*$ of all the materials tested. Moreover, through-the-thickness strength testing failed to produce a delamination in this material. Using this $Q^*$ parameter to rate the materials, the stitched uniweaves, toughened epoxy tapes, and OS-2 through-the-thickness orthogonal interlock weave were the most damage resistant.

## References

[1]    Jackson, W. C. and Martin, R. H., "An interlaminar Tensile Strength Specimen," Composite Materials: Testing and Design (Eleventh Volume), ASTM STP 1206, E. T. Camponeschi, Jr., Ed., American Society for Testing and Materials, Philadelphia, December 1993, pp. 333-354.

[2]    Jackson, W. C. and Ifju, P. G. "Through-the-Thickness Tensile Strength of Textile Composites," Composite Materials: Testing and Design (Twelfth Volume), ASTM STP, C. R. Saff and R. B. Deo, Eds., American Society for Testing and Materials, Philadelphia. (submitted for publication)

[3]    Falcone, A., Dursch, H, Nelson, and Avery, W., "Resin Transfer Molding of Textile Composites," NASA CR 191505, July 1993.

[4]    Lekhnitskii, S.G., "Anisotropic Plates," Gordon and Breach Science Publishers, New York, 1968, pp. 95-101.

[5]    Ifju, P. G.; Masters J. E.; and Jackson W. C. "Using Moire Interferometry to Aid in Standard Test Method Development for Textile Composite Materials," submitted for publication to Journal of Composites Science and Technology.

[6]    Jackson, W. C. and Poe, C. C. Jr., "The Use of Impact Force as a Scale Parameter for the Impact Response of Composite Laminates," Journal of Composites Technology & Research, Vol. 15, No. 4, Winter 1993, pp. 282-289.

[7]    Sjöblom, Peter: Simple Design Approach Against Low-Velocity Impact Damage. 32nd International SAMPE Symposium, April 6-9, 1987, pp. 529-539.

[8]    Elber, W.: Failure Mechanics in Low-Velocity Impacts on Thin Composite Plates. NASA TP 2152, May 1983.